https://doi.org/10.5194/egusphere-2026-4328
Preprint. Discussion started: 24 August 2026

Evolution and drivers of urban–suburban ozone contrasts in China during 2013–2020

Ning Yang[1], Qiaoqiao Wang[1], Nan Ma[1], Guangjin Liu[1], Zheng Yang[1], Yuanwei Zhong[1], Zechao Hu[1], Yaqing Zhou[1], Jiangchuan Tao[1], Juan Hong[1], Yafang Cheng[2], Hang Su[3]

[1]College of Environment and Climate, Institute for Environmental and Climate Research, Guangdong-Hongkong-Macau Joint Laboratory of Collaborative Innovation for Environmental Quality, Jinan University, Guangzhou 511443, China
[2]Aerosol Chemistry Department, Max Planck Institute for Chemistry, Mainz 55128, Germany
[3]State Key Laboratory of Atmospheric Environment and Extreme Meteorology, Institute of Atmospheric Physics, Chinese Academy of Sciences, Beijing 100029, China

Correspondence to: Qiaoqiao Wang (qwang@jnu.edu.cn)

Abstract. Urban–suburban surface ozone (O_3) differences provide valuable information for understanding the spatial response of O_3 to emission reductions, yet their long-term evolution across China remains poorly understood. Here, we combined surface observations with GEOS-Chem simulations to investigate summertime urban–suburban O_3 contrasts across China during 2013–2020. Urban and suburban areas were reclassified using a population density threshold, and the contributions of meteorology (Met), anthropogenic emissions (Anth), and biogenic VOCs emissions (Biog) were quantified using sensitivity simulations. Reclassification enlarged the urban–suburban O_3 contrast in eastern China but reversed the interpretation in western China from urban O_3 enhancement to persistent suburban enhancement. Suburban monitoring sites also underestimated regional suburban O_3 trends, indicating limited spatial representativeness. Nationally, suburban O_3 increased faster than urban O_3 after 2017, weakening the urban–suburban gradient. Attribution revealed distinct controlling mechanisms. In eastern urban areas, Anth enhanced O_3 during 2013–2017 under VOCs-limited conditions but became suppressive by 2020 as chemistry shifted toward transitional regimes, while Met dominated recent increases. In eastern suburban areas, Met was the primary driver, whereas Anth consistently suppressed O_3 under predominantly NO_x-limited conditions. In western China, weak Anth and Biog contributions made Met the dominant driver in both urban and suburban areas. Case studies further demonstrate substantial regional heterogeneity in driver contributions and O_3 sensitivity regimes. These findings highlight the importance of robust urban–suburban classification, representative monitoring, and region-specific O_3 drivers for developing effective mitigation strategies.

1 Introduction

Surface ozone (O_3) has become an increasingly important air-quality challenge in China as fine particulate matter ($PM_{2.5}$) has declined under successive clean-air actions (Geng et al., 2024; Zhang et al., 2019). Unlike primary pollutants, O_3 is formed through nonlinear photochemical reactions involving nitrogen oxides (NOx), anthropogenic volatile organic compounds

(AVOCs), biogenic volatile organic compounds (BVOCs), and meteorological conditions. This nonlinearity makes O_3 responses to emission controls spatially heterogeneous, particularly between urban areas, where anthropogenic emissions are concentrated, and suburban areas, which are more strongly affected by vegetation and regional transport (Wang et al., 2017). Understanding how urban–suburban O_3 contrasts evolve is therefore essential for evaluating the effectiveness of O_3 control strategies and for avoiding spatially biased policy conclusions.

Previous studies have shown that recent O_3 trends in China were shaped by both anthropogenic emission changes and meteorological variability (Li et al., 2020; Liu et al., 2023), but conclusions regarding urban–suburban differences remain inconsistent. Some studies reported a widening urban–suburban O_3 gap, whereas others suggested comparable trends between urban and non-urban areas (Liu and Wang, 2020; Xing et al., 2022; Dai et al., 2024; Wang et al., 2022b). One key source of uncertainty is the definition of urban and suburban areas. Monitoring-site classifications used in long-term networks may become outdated under rapid urban expansion, while alternative approaches based on population density, nighttime light, or urban spatial structure can assign substantially different samples to urban and suburban categories, which can strongly affect inferred O_3 trends and their urban–suburban contrasts.

Beyond classification uncertainty, the mechanisms controlling urban–suburban O_3 differences remain insufficiently constrained. Urban regions in eastern China have often been characterized by VOCs-limited or transitional O_3 formation, so NOx reductions can either enhance O_3 by weakening NO titration or suppress O_3 after the chemical regime shifts toward transitional or NOx-limited conditions (Xue et al., 2026; Wang et al., 2021). Suburban regions generally have lower NOx and AVOCs emissions but comparable or stronger influences from BVOCs and regional transport, which may lead to different O_3 formation regimes and different responses to the same emission reductions (Gao et al., 2025; Xu et al., 2025). Meteorological conditions further modulate these responses through changes in temperature, radiation, dispersion, and biogenic emissions (Wang et al., 2022a; Yan et al., 2024). A systematic attribution of meteorological conditions, anthropogenic emissions, and BVOCs emissions is therefore needed to explain why urban and suburban O_3 trends can diverge across regions and over time.

Here, we investigate summertime urban–suburban O_3 contrasts in China during 2013–2020 by combining surface observations with GEOS-Chem simulations. We first reclassify urban and suburban monitoring sites using high-resolution population density data to evaluate how classification choices influence inferred O_3 trend differences. We then analyze the evolution of urban–suburban O_3 trends at national and regional scales and quantify the relative contributions of meteorological conditions, anthropogenic emissions, and BVOCs emissions using sensitivity simulations. Finally, we examine the Jing-Jin-Ji (JJJ) and Yangtze River Delta (YRD) regions as case studies to link urban–suburban O_3 trends with changes in O_3 formation regimes. This study highlights the importance of classification, site representativeness, and chemical-regime evolution in interpreting urban–suburban O_3 differences, and provides a basis for more spatially targeted O_3 mitigation strategies in China.

https://doi.org/10.5194/egusphere-2026-4328
Preprint. Discussion started: 24 August 2026

2 Data and methods

2.1 GEOS-Chem model

We used the GEOS-Chem chemical transport model (version 13.3.2; www.geos-chem.org), driven by assimilated meteorological fields from the NASA Global Modeling and Assimilation Office (GEOS-FP), to simulate the spatiotemporal distributions of O_3 and related chemical species, including formaldehyde (HCHO) and nitrogen dioxide (NO_2) in China. The simulations were conducted using the nested-grid configuration over Asia at a horizontal resolution of 0.25° latitude × 0.3125° longitude, with 47 vertical layers extending from the surface to the stratosphere. Dynamic boundary conditions were provided by a global GEOS-Chem simulation at a horizontal resolution of 4° × 5°. A one-month spin-up was applied before the continuous simulations for 2013–2020.

The simulation included fully coupled HO_x-NO_x-VOCs-O_3-aerosol chemistry, with approximately 300 chemical species and more than 400 kinetic and photolytic reactions (Dai et al., 2024; Li et al., 2019; Pye et al., 2010). Global anthropogenic emissions were obtained from version 2 of the Community Emissions Data System (CEDS) inventory (Hoesly et al., 2018), with emissions over China replaced by version 1.4 of the Multi-resolution Emission Inventory for China (MEIC) (Li et al., 2019; Zheng et al., 2018). The anthropogenic intermediate-volatility organic compounds (IVOCs) emission inventory developed by Yang et al. (2025) was also incorporated. Biomass burning emissions were taken from the Global Fire Emissions Database version 4 (GFED4) with a 3-hour temporal resolution (Andreae, 2019; Giglio et al., 2013). BVOCs emissions were calculated online using the Model of Emissions of Gases and Aerosols from Nature version 2.1 (MEGAN2.1) (Guenther et al., 2012).

To quantify the relative contributions of anthropogenic emissions, BVOCs emissions, and meteorological conditions to O_3 changes, we conducted two sensitivity simulations in addition to the base simulation (Table 1). The FixA and FixAB simulations used the same model configuration as the base simulation but differed in their emission settings. In FixA, anthropogenic emissions were fixed at their 2013 levels, whereas in FixAB, both anthropogenic emissions and BVOCs emissions were fixed at their 2013 levels. The difference between the base and FixA simulations was used to quantify the effect of changes in anthropogenic emissions, and the difference between FixA and FixAB quantifies the effect of changes in BVOCs emissions. The remaining difference, represented by FixAB relative to the baseline simulation, was attributed to meteorological influences on O_3 concentrations. Here, the meteorological contribution includes only the direct effects of meteorological variability on transport, dispersion, deposition, and chemistry, and does not include meteorology-induced changes in BVOCs emissions, which are quantified separately as described above.

Table 1. Configurations of GEOS-Chem simulations in this study.

Scenario	Simulated years	Anthropogenic emissions	Biogenic VOCs emissions	Meteorology
Base	2013–2020	Year-specific	Year-specific	Year-specific
FixA	2017, 2019, 2020	Fixed at 2013 level	Year-specific	Year-specific
FixAB	2017, 2019, 2020	Fixed at 2013 level	Fixed at 2013 level	Year-specific

Owing to computational constraints, sensitivity simulations were only conducted for 2017, 2019, and 2020. These years represent three distinct stages of recent emission changes in China. Specifically, 2017 corresponds to the late stage of the Air Pollution Prevention and Control Action Plan, when emission reductions were ongoing; 2019 represents the full implementation of the Blue Sky Defense Battle, during which emission controls and structural adjustments were strengthened with greater emphasis on VOCs reduction (Guo et al., 2024); and 2020 captures the COVID-19 lockdown period, when abrupt activity changes caused short-term reductions in anthropogenic emissions. These selected years allow us to compare how anthropogenic emissions, BVOCs emissions, and meteorological conditions affected O_3 and its urban–suburban contrasts under different activity and control regimes.

2.2 O_3 formation regime classification

The ratio of HCHO to NO_2 ($HCHO/NO_2$, hereafter FNR) was used as an indicator of O_3 formation sensitivity (Wang et al., 2021; Zheng et al., 2023; Jin et al., 2020). Following previous studies, we identified O_3 formation regimes by relating FNR to the ozone exceedance probability (OEP). FNR values were grouped into intervals of 0.1, and OEP was calculated for each interval as the probability that O_3 concentrations exceeded 160 μg m^{-3}. A sixth-order polynomial function was then fitted to the OEP-FNR relationship. The FNR corresponding to the maximum fitted OEP was defined as the critical point at which O_3 production is most efficient. The FNR range where the fitted OEP greater than or equal to 90% of the peak value was defined as the transitional regime. FNR values below and above this range were classified as VOCs-limited and NO_x-limited regimes, respectively. To estimate uncertainty in the critical FNR, we applied bootstrap resampling with 1000 iterations and defined the uncertainty range as the peak position ±2 standard deviations of the bootstrap estimates.

2.3 Urban–suburban classification

We used population density to classify urban and suburban areas because it directly reflects the intensity of human activity and is widely used to characterize urban spatial structure (Wang et al., 2024). A 1 km × 1 km population density dataset was obtained from the Resource and Environment Science and Data Center (RESDC; https://www.resdc.cn/). To derive a threshold suitable for national-scale urban–suburban classification, we first referred to the city-size classification standard issued by the State Council of China, which categorizes cities by urban population into small cities (<5 million), medium cities (5–10 million), large cities (10–50 million), very large cities (50–100 million), and megacities cities (>10 million) (https://www.gov.cn/zhengce/content/2014-11/20/content_9225.htm). Using city population and urban area statistics from the China Statistical Yearbook for 2015 (https://data.cnki.net/), we calculated the mean population density for each city category, yielding values of 106, 281, 342, 564, and 889 persons km^{-2}, respectively (Table S1).

We further compiled reported suburban population densities for four representative Chinese cities (Beijing, Tianjin, Ningbo, and Shenzhen; Table S1). These cities are economically developed and generally exhibit more intensive suburban development than less-developed regions, especially in central and western China. To avoid selecting a threshold that is overly influenced by highly urbanized suburban conditions, we used the minimum reported suburban density for each city

https://doi.org/10.5194/egusphere-2026-4328
Preprint. Discussion started: 24 August 2026

and then averaged these four minimum values to represent a conservative suburban benchmark. This benchmark was compared with the mean population densities of the five city-size categories, and the category with the smallest difference was selected as the classification threshold. Based on this procedure, the mean population density of large cities (342 persons km^{-2}) was selected as the threshold for distinguishing urban and suburban areas. This threshold is anchored in the national city-size classification system while also being constrained by reported suburban population densities, thereby balancing national comparability with realistic suburban conditions. Figure 1 shows the resulting classification of model grid cells and monitoring sites across mainland China. Compared with the classification adopted by the China National Environmental Monitoring Centre (CNEMC), the population density-based classification reassigned 156 originally suburban sites to urban sites, mainly in economically developed regions such as the JJJ, YRD, and PRD. and reassigned 145 originally urban sites to suburban sites, mostly in central and western China.

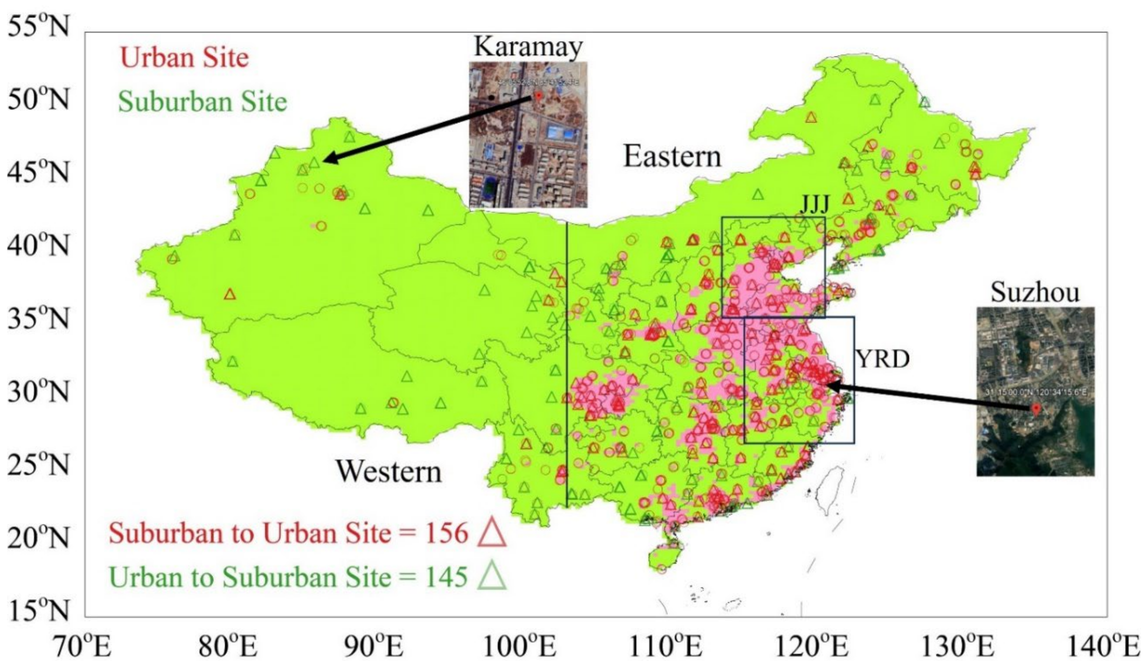

Figure 1. Spatial distribution of urban (red) and suburban (green) areas over mainland China based on population density averaged at the model grid resolution. Monitoring site classifications are also shown, with circles indicating sites consistent with the original urban-suburban classification from the China National Environmental Monitoring Center and triangles denoting sites with revised classification based on population density. Point-location maps of Karamay and Suzhou, derived from Google Maps, are presented to demonstrate representative reclassification cases under the original and revised classification schemes.

https://doi.org/10.5194/egusphere-2026-4328
Preprint. Discussion started: 24 August 2026

2.4 Observed surface O_3

MDA8 O_3 concentrations were obtained from the CNEMC (https://www.cnemc.cn/). To ensure data quality, only monitoring sites with annual missing rates below 20% were retained. To match the model resolution and reduce sampling bias, observations from multiple monitoring sites within the same grid cell were averaged before comparison with simulations. When more than one monitoring site was located in a grid cell, the grid-cell site type was determined by majority rule. For example, a grid cell containing two urban sites and one suburban site was classified as urban. Grid cells for which the aggregated monitoring-site classification was inconsistent with the population density-based model-grid classification were excluded from subsequent model-observation comparisons.

The number and spatial coverage of O_3 monitoring sites were substantially lower during 2013–2014 than in later years. Trend estimates based on observations over the full 2013–2020 period may therefore be affected by sampling changes. We thus used observations from 2015–2020, including 1450 monitoring sites, to evaluate the model performance in reproducing recent O_3 trends.

3 Results and Discuss

3.1 Influence of Urban–Suburban Classification on Estimated O_3 Trend Differences

The estimated urban–suburban O_3 contrast was strongly affected by the classification method used to define urban and suburban sites (Fig. 2 and S1). Under the original CNEMC classification (the old classification), summertime O_3 increased in both urban and suburban areas during 2015–2020, but the increase was faster at urban sites than at suburban sites (1.5 vs. 0.88 ppb yr^{-1}), yielding an urban–suburban trend difference of 0.62 ppb yr^{-1}. In eastern China, urban O_3 remained consistently higher than those in suburban areas throughout the study period. Consequently, the faster urban increase further enlarged the urban–suburban O_3 concentration difference from 2.5 ppb in 2015 to 5.5 ppb in 2020. After applying the population density-based classification (the new classification), this contrast became more pronounced in eastern China. The urban O_3 trend in eastern China increased slightly to 1.7 ppb yr^{-1}, whereas the suburban trend decreased to 0.77 ppb yr^{-1}, increasing the urban–suburban trend difference from 0.70 ppb yr^{-1} to 0.93 ppb yr^{-1}. Because urban O_3 concentrations were already higher than suburban concentrations in eastern China, this adjustment enlarged the estimated urban–suburban concentration gap in 2020 from 5.5 ppb under the old classification to approximately 12 ppb under the new classification.

https://doi.org/10.5194/egusphere-2026-4328
Preprint. Discussion started: 24 August 2026

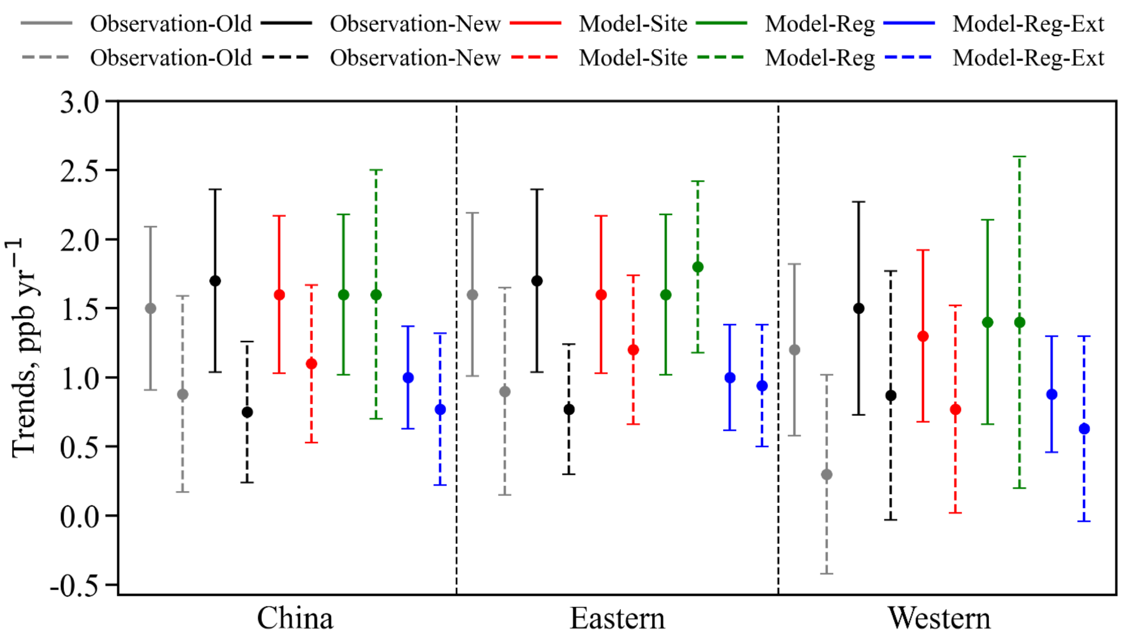

Figure 2. Observed and simulated summer O_3 trends averaged over China and subregions (Eastern and Western) from 2015 to 2020. Solid and dashed lines denote urban and suburban areas, respectively. Observations using the old and new urban-suburban classifications are shown in gray and black. Model results based on the new classification include outputs sampled at observation sites (red) and over all grid cells (green). Model results over all grids extend to the period of 2013–2020 are also shown (blue).

This change mainly reflects the reassignment of monitoring sites whose surrounding environments have become more urbanized (Fig. 1). For example, the Suzhou site was classified as suburban under the original CNEMC scheme, but its O_3 concentration level and trend were much closer to those of urban sites in eastern China (Fig. S1). Retaining such sites in the suburban category would overestimate suburban O_3 concentrations and growth rates, thereby weakening the apparent urban–suburban contrast. The new classification is therefore more consistent with rapid urban expansion in eastern China, where some sites originally located in suburban environments are now strongly influenced by urban emissions (Gao et al., 2020).

In western China reclassification had a different but equally important effect. Under the original CNEMC classification, urban O_3 increased faster than suburban O_3, and the urban–suburban concentration difference shifted from −1.5 ppb in 2015 to +2.7 ppb in 2020, suggesting a reversal from lower urban O_3 to higher urban O_3. After applying the population density-based classification, however, several sites originally classified as urban were reassigned to suburban areas because their population density and surrounding environments were more consistent with suburban conditions (e.g. Karamay site in Fig. 1). This reassignment lowered the mean O_3 concentration of urban sites and increased that of suburban sites. Although O_3 still increased faster in urban areas than in suburban areas under the new classification (1.5 vs. 0.87 ppb yr–1), urban O_3 concentrations remained lower than suburban concentrations throughout the study period. As a result, the urban–suburban

https://doi.org/10.5194/egusphere-2026-4328
Preprint. Discussion started: 24 August 2026

concentration contrast weakened in magnitude, from −8.7 ppb in 2015 to −6.5 ppb in 2020, but did not change sign. The new classification therefore changes the interpretation for western China from an apparent urban O_3 exceedance to a persistent suburban O_3 enhancement with a narrowing urban–suburban gap.

These results highlight the importance of the population-density threshold used for urban–suburban classification. Different thresholds change which monitoring sites or model grid cells are assigned to urban and suburban categories, and can therefore alter both the magnitude and direction of inferred O_3 contrasts. For example, Wang et al. (2022b) used a much higher population-density threshold of 2500 persons km^{-2}, which classified a larger fraction of moderately urbanized areas as suburban. As a result, grid cells with effectively urban characteristics were partly included in the suburban category, leading to higher suburban mean O_3 concentrations (53 ppb) and faster suburban O_3 increases. This threshold choice ultimately produced similar urban and suburban O_3 trends (1.8 vs. 1.7 ppb yr^{-1}), whereas our lower threshold, constrained by national city-size categories and reported suburban densities, separates these moderately urbanized areas from truly suburban environments and yields a clearer urban–suburban contrast. Thus, the definition of the classification threshold is central to interpreting urban–suburban O_3 differences and to reconciling apparently inconsistent conclusions among previous studies. Unless otherwise specified, all subsequent analyses are based on the population density-based classification developed in this study.

3.2 Model Evaluation and Site Representativeness

Figures 2 and 3 compare the observed and simulated summertime O_3 concentrations at urban and suburban sites based on the population density-based classification. The model generally reproduces the observed interannual variability of O_3 in both environments, although it shows a systematic positive bias in annual mean concentrations. For urban sites, the normalized mean bias (NMB) ranges from 20% to 29%, with correlation coefficients (r) of 0.70–0.73. For suburban sites, the NMB is slightly lower (16%–21%), but the temporal correlations are weaker (r = 0.58–0.61). Despite these biases, the simulated trends are broadly consistent with observations and capture the faster O_3 increase at urban sites. However, the simulated suburban trend is higher than the observed trend, particularly in eastern China, where the model-derived suburban increase is about 1.6 times the observed value. As a result, the model underestimates the site-based urban–suburban trend contrast (0.50 vs. 0.95 ppb yr–1).

This apparent model–observation discrepancy is closely related to the limited representativeness of suburban monitoring sites. Suburban areas cover much larger and more heterogeneous spaces than urban areas and are affected by a combination of local BVOCs emissions, regional transport, land-cover differences, and gradients in anthropogenic emissions(Li et al., 2025; Cao et al., 2022). The existing suburban monitoring sites are relatively sparse and cannot fully capture this spatial heterogeneity. To evaluate this effect, we compared site-averaged model results with regional mean concentrations calculated from all model grid cells classified as urban or suburban. For urban areas, O_3 trends derived from monitoring-site averages and regional grid-cell averages were nearly identical, indicating that urban sites are relatively representative of broader urban conditions. In contrast, suburban regional mean trends (1.4–1.8 ppb yr–1) were substantially higher than those

https://doi.org/10.5194/egusphere-2026-4328
Preprint. Discussion started: 24 August 2026

derived from suburban site averages (0.77–1.2 ppb yr–1). The magnitude of this site–region difference is comparable to the difference between modeled and observed suburban trends, suggesting that the apparent overestimation of suburban O_3 trends by the model is largely attributable to sampling limitations rather than model performance alone.

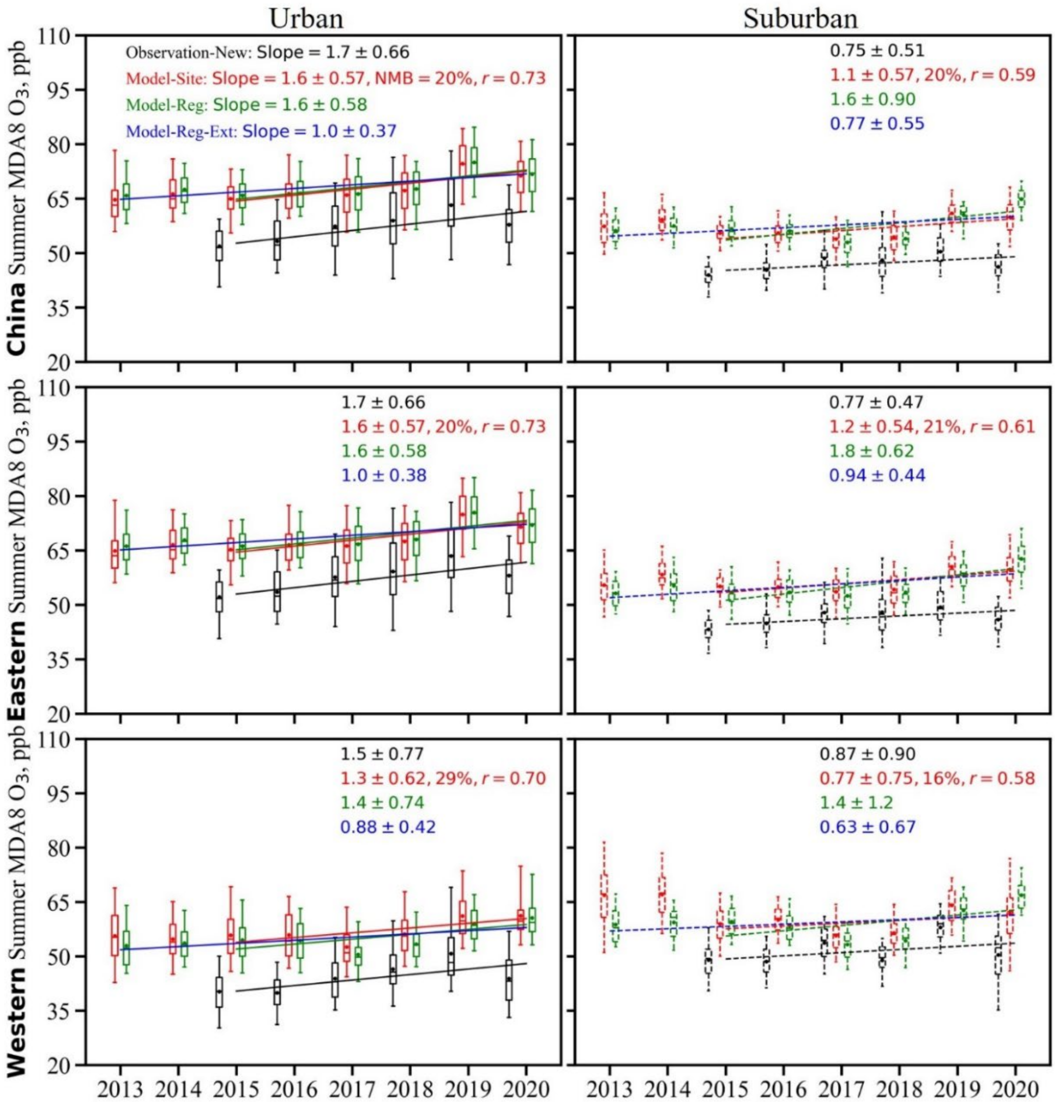

225 **Figure 3.** Observed and simulated trends in summer O_3 concentrations at urban (left column) and suburban (right column) sites in China and subregions (Eastern and Western) from 2015 to 2020, based on the observed-new (black), model-site (red), model-reg (green) and model-reg-ext (blue). The fitted lines indicate linear trends, with corresponding slopes, normalized mean bias (NMB), and correlation coefficients (r) values annotated. Simulated trends from 2013 to 2020 are also shown in blue.

The lack of suburban site representativeness has important implications for interpreting urban–suburban O_3 contrasts. If only monitoring-site averages are used, the urban–suburban trend difference may be overestimated because the sparse suburban sites do not adequately represent the faster O_3 increases occurring across broader suburban regions. When regional grid-cell averages are used instead, the inferred urban–suburban contrast becomes smaller, and in eastern China the sign of the trend difference even reverses, with suburban O_3 increasing slightly faster than urban O_3. Therefore, subsequent analyses are based on regional mean concentrations rather than site-based averages to reduce the influence of uneven monitoring-site coverage. This result also highlights the need for denser and more spatially representative suburban O_3 monitoring networks in China.

3.3 Simulated Urban–Suburban Differences in Regional Means

Figures 2 and 3 show a clear stage-dependent evolution of summertime O_3 in China during 2013–2020. At the national scale, O_3 showed no statistically significant increase in either urban or suburban areas during 2013–2016, but increased rapidly during 2017–2020. The increase was stronger in suburban areas than in urban areas (4.3 vs. 2.4 ppb yr–1), causing the national urban–suburban O_3 difference to decrease from 9.6 ppb in 2013 to 6.8 ppb in 2020. This weakening of the urban–suburban gradient indicates that suburban O_3 has increased more rapidly in recent years, even though urban concentrations remained higher on average. The regional patterns differed between eastern and western China. In eastern China, urban O_3 concentrations were consistently higher than suburban concentrations, but the faster increase in suburban O_3 narrowed the urban–suburban gap over time. In western China, urban O_3 concentrations were generally lower than suburban concentrations throughout the study period, and the faster suburban increase further strengthened the suburban O_3 enhancement. These results suggest that urban–suburban O_3 contrasts are not fixed spatial gradients, but evolve with regional emission structures, meteorological conditions, and O_3 formation regimes.

A notable feature is the decline in summertime urban O_3 in eastern China from 2019 to 2020, which is reproduced by both observations and simulations. This decrease is associated with reductions in NOx and AVOCs emissions during the COVID-19 lockdown period, with NOx and AVOCs emissions decreasing by 3.0% and 3.1%, respectively, relative to 2019 (Fig. S2). More broadly, sustained NOx reductions during 2013–2019 gradually shifted summertime O_3 formation in many eastern Chinese cities from VOCs-limited conditions toward transitional or even NOx-limited regimes. Under these evolving chemical conditions, further NOx reductions increasingly suppressed O_3 production, contributing to the observed urban O_3 decline in 2020 (Xue et al., 2026; Wang et al., 2022a).

3.3.1 Contributions of meteorology, anthropogenic emissions, and BVOCs emissions

Figure 4 decomposes O_3 changes into contributions from meteorological conditions (Met), anthropogenic emissions (Anth), and BVOCs emissions (Biog). The relative importance of these drivers differed strongly between urban and suburban areas. In eastern urban areas, the dominant driver shifted from Anth during 2013–2017 to Met during 2018–2020. Between 2013 and 2017, Anth enhanced O_3 by about 1.4%, while the contribution of Met was weak (~0.20%). During 2019–2020, however,

https://doi.org/10.5194/egusphere-2026-4328
Preprint. Discussion started: 24 August 2026

Met enhanced O_3 by approximately 11%–14% and became the dominant driver, whereas the contribution of Anth weakened and became negative in 2020 (−0.84%). Biog consistently exerted a weak suppressing effect on eastern urban O_3.

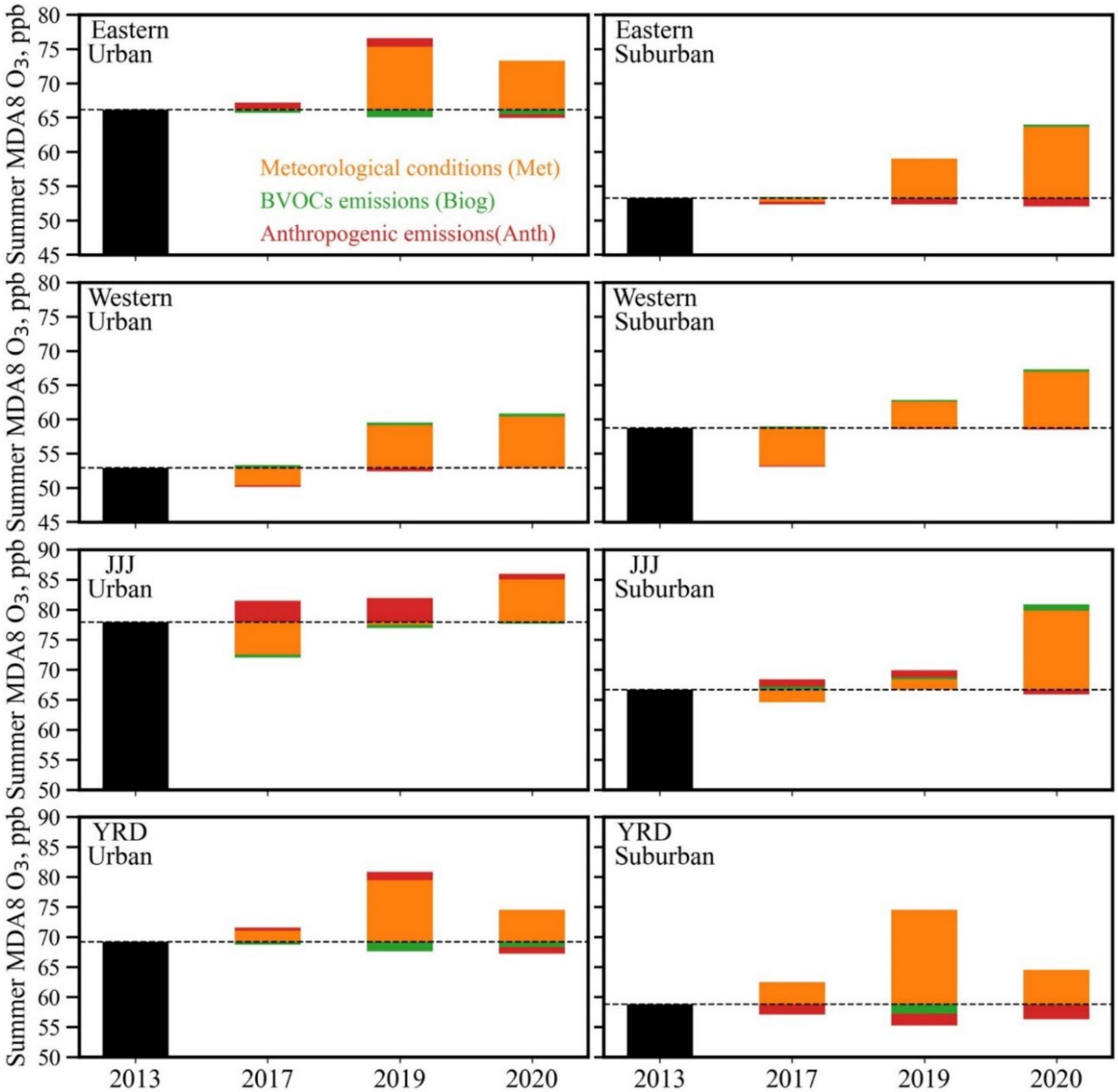

Figure 4. Contributions of meteorological conditions (Met), biogenic emissions (Biog), and anthropogenic emissions (Anth) to the changes in summer O_3 concentrations during 2013–2020 at urban and suburban sites in Eastern, Western, JJJ, and YRD. Black bar represents simulated O_3 concentrations in 2013, while colored bars represent changes due to different drivers in 2017, 2019, and 2020 based on sensitivity simulations.

The stage-dependent effect of Anth was closely linked to concurrent changes in precursor emissions and the associated shift in O_3 sensitivity regimes. During 2013–2017, NOx emissions decreased continuously by approximately 20%, while AVOCs and BVOCs emissions increased slightly by about 7.7% and 0.56%, respectively (Fig. S2 and S3). These changes

https://doi.org/10.5194/egusphere-2026-4328
Preprint. Discussion started: 24 August 2026

increased the $HCHO/NO_2$ ratio, which reached approximately 1.0 in 2018. The positive relationship between O_3 and $HCHO/NO_2$ suggests that eastern urban areas were predominantly VOCs-limited during this early period. Under this regime, increasing AVOCs enhanced radical production and O_3 formation, while decreasing NOx weakened NO–O_3 titration. Together, these effects explain why Anth enhanced urban O_3 during 2013–2017. After 2017, continued NOx reductions, together with a decline in VOCs emissions （-5.5% and -15% for AVOCs and BVOCs during 2017-2020）, shifted urban O_3 formation away from strongly VOCs-limited conditions toward the transitional regime. Consequently, the contribution of Anth weakened after 2017 and became negative in 2020 (−0.84%).

Similarly, the small change in BVOCs emissions during 2013–2017 led to a negligible Biog contribution, whereas BVOCs decreases in 2019 and 2020 produced weak O_3 reductions. Overall, eastern urban O_3 changed from being mainly emission-driven in the early period to being more strongly modulated by meteorology in the later period, while the effect of anthropogenic emissions shifted from enhancement to suppression as chemical sensitivity evolved.

In contrast, O_3 variability in eastern suburban areas was dominated by Met throughout the study period. During 2019–2020, Met enhanced suburban O_3 by approximately 11%–19%, comparable to or larger than its contribution in urban areas, suggesting that suburban O_3 is strongly influenced by large-scale meteorological variability. Furthermore, Anth consistently suppressed O_3 in eastern suburban areas. This urban–suburban difference reflects their distinct precursor environment and O_3 sensitivity. Suburban areas had much lower NOx and AVOCs emissions than urban areas, whereas BVOCs emission intensities were comparable to those in urban environments. As a result, both NO_2 and HCHO concentrations were lower in suburban areas, but the $HCHO/NO_2$ ratio remained much higher, generally exceeding 2. These high FNR values indicate that eastern suburban O_3 formation was predominantly NOx-limited throughout the study period. This consistent with previous finding that most regions in China, except for urban cores, are generally NOx-limited (Guo et al., 2019; Li et al., 2021). Under NOx-limited conditions, reductions in NOx emissions directly suppress O_3 production. Therefore, unlike eastern urban areas where Anth first enhanced and later suppressed O_3, Anth consistently exerted a negative effect on eastern suburban O_3. This contrast shows that the same regional anthropogenic emission reductions can produce different O_3 responses in urban and suburban environments because their chemical regimes differ.

The role of Biog further illustrates the importance of suburban environments. In eastern suburban areas, BVOCs emissions were comparable in intensity to urban areas despite lower NOx and AVOCs emissions. Nevertheless, because suburban O_3 formation was mainly NOx-limited, changes in BVOCs alone had a smaller overall effect than changes in NOx or Met. This suggests that BVOCs are not the dominant driver of suburban O_3 changes at the regional mean scale. However, they can still modulate O_3 formation locally by increasing reactive VOCs oxidation and producing RO_2 and HO_2 radicals, which accelerate the conversion of NO to NO_2 when sufficient NOx is available Wu et al. (2020). Consistent with this mechanism, Biog contributed weakly to suburban O_3 formation only in 2020, when BVOCs emissions were slightly increased in some suburban areas.

Western China exhibited a different driver structure from eastern China. O_3 variability was dominated by Met in both urban and suburban areas, while Anth remained weak and generally negative. Biog exerted a weak positive influence, but its

https://doi.org/10.5194/egusphere-2026-4328
Preprint. Discussion started: 24 August 2026

contribution was small because BVOCs emission intensities in western suburban areas were less than 15% of those in eastern suburban areas. Compared with eastern urban areas, western urban areas had much lower NOx, AVOCs, and BVOCs emissions, and stronger solar radiation likely favored secondary HCHO formation (Yang et al., 2020), resulting in higher $HCHO/NO_2$ ratios and more NOx-limited conditions. Consequently, reductions in NOx emissions tended to suppress O_3, similar to eastern suburban areas. Under these low-emission conditions, Anth and Biog had only weak effects on O_3, while Met dominated O_3 variability in both urban and suburban areas. The urban–suburban difference in driver contributions was therefore much smaller in western China than in eastern China.

Overall, the urban–suburban differences in O_3 drivers can be explained by both emission contrasts and chemical sensitivity. In eastern urban areas, early-stage VOCs-limited chemistry allowed NOx reductions to increase O_3 by weakening NO–O_3 titration, while increasing AVOCs further promoted radical recycling and O_3 production. As NOx emissions continued to decline and VOCs growth slowed or reversed after 2017, urban O_3 formation moved toward the transitional regime, causing Anth to shift from an enhancing to a suppressing influence. In eastern suburban areas, persistent NOx-limited conditions made NOx reductions consistently suppress O_3, while Met remained the dominant driver. In western China, low precursor emissions made Met the primary control in both urban and suburban areas. In western China, both urban and suburban areas were characterized by lower anthropogenic and BVOCs emissions and more NOx-limited conditions, which lead to dominated driver of Met and much less pronounced urban–suburban differences in driver responses than in eastern China.

3.3.2 Case Studies: JJJ and YRD

The JJJ and YRD regions were selected to further illustrate how urban–suburban differences in O_3 formation regimes regulate the response of O_3 to Met, Anth, and Biog. In JJJ, urban O_3 increased more slowly than suburban O_3 during 2013–2020 (1.0 vs. 1.4 ppb yr^{-1}), so the urban–suburban O_3 difference gradually decreased despite persistently higher urban O_3 concentrations. In contrast, YRD showed a faster increase in urban O_3 than suburban O_3 (0.94 vs. 0.70 ppb yr^{-1}), leading to a widening urban–suburban contrast. These different trends were closely linked to regional differences in chemical-regime evolution and driver contributions.

Figure 4 also illustrates the dominant drivers of O_3 variability in JJJ and YRD at different stages. In urban JJJ, the dominant driver shifted markedly over time, from Met during 2013–2017 to Anth in 2019, and then back to Met in 2020. In contrast, suburban JJJ was consistently dominated by Met. Anth generally contributed positively to O_3 in both urban and suburban areas, with the only exception occurring in suburban areas in 2020. In the YRD, O_3 changes were primarily controlled by Met throughout the study period. The contribution of Anth in urban areas shifted from positive to negative, whereas in suburban areas Anth consistently suppressed O_3. The contribution of Biog was generally smaller than those of Met and Anth in both JJJ and YRD, but it still modulated O_3 responses where BVOCs changes interacted with local chemical regimes. Overall, Fig. 4 shows that the contrasting urban–suburban O_3 trends in JJJ and YRD were shaped not only by changes in O_3 concentrations, but also by differences in driver contributions and their underlying O_3 sensitivity regimes.

https://doi.org/10.5194/egusphere-2026-4328
Preprint. Discussion started: 24 August 2026

The estimated FNR ranges for the transitional O_3 formation regime were 0.55–1.3 in JJJ and 0.75–1.5 in YRD (Fig. S4). Values above these ranges were classified as NOx-limited, whereas values below them were classified as VOCs-limited. As shown in Fig. 5, O_3 formation in urban JJJ in 2013 was mainly VOCs-limited or transitional. Between 2013 and 2017, NOx emissions decreased by about 20%, AVOCs emissions increased by 4.1%, and BVOCs emissions changed little (Fig. 6 and S5). These changes decreased NO_2 by 6.5%, increased HCHO by 3.3%, and raised the mean FNR from 0.49 to 0.56, shifting parts of the region from VOCs-limited toward transitional conditions (particularly in northern Beijing and northwestern Shandong). Under VOCs-limited chemistry, both increasing AVOCs and decreasing NOx could enhance O_3, explaining the positive contribution of Anth during the early period. After 2017, NOx declined faster than VOCs, and parts of urban JJJ shifted back toward VOCs-limited conditions, particularly along the Shandong–Hebei border. In these areas, increased AVOCs and decreased NOx continued to promote O_3 formation in 2019 and 2020.

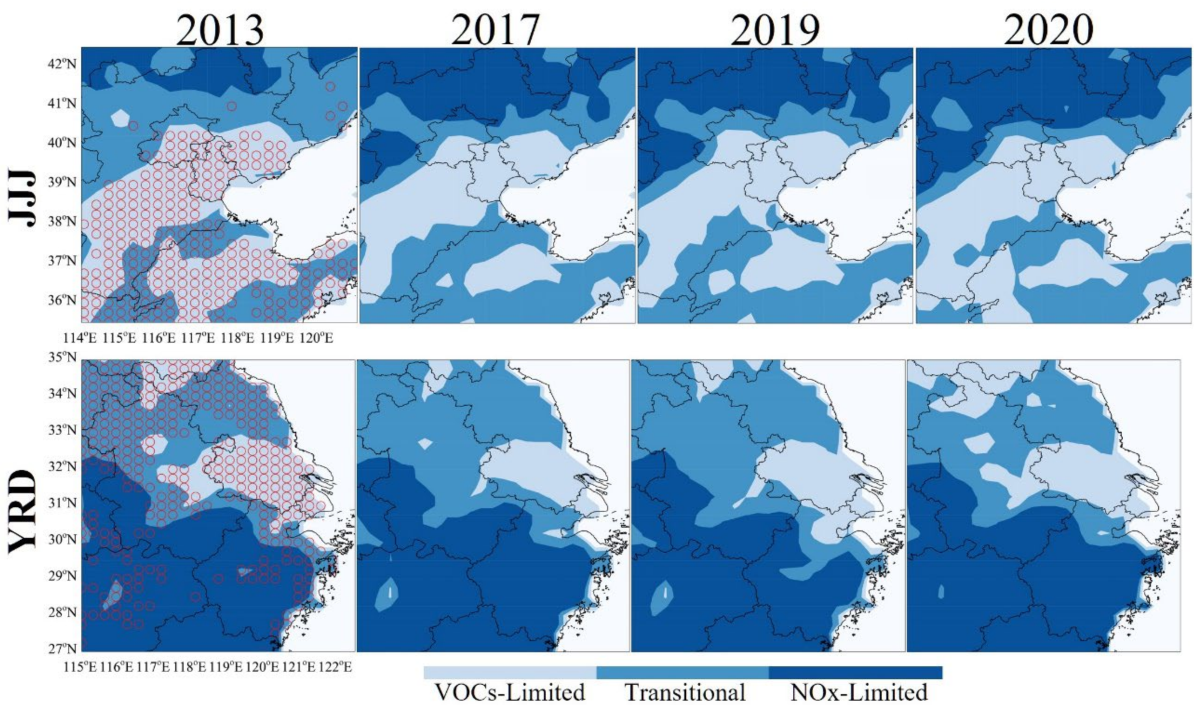

Figure 5. Photochemical regime classification over JJJ and YRD in the summer in 2013, 2017, 2019 and 2020 based on $HCHO/NO_2$ concentration ratio (FNR). In the 2013 panel, red circles represent urban areas, and the rest are classified as suburban.

https://doi.org/10.5194/egusphere-2026-4328
Preprint. Discussion started: 24 August 2026

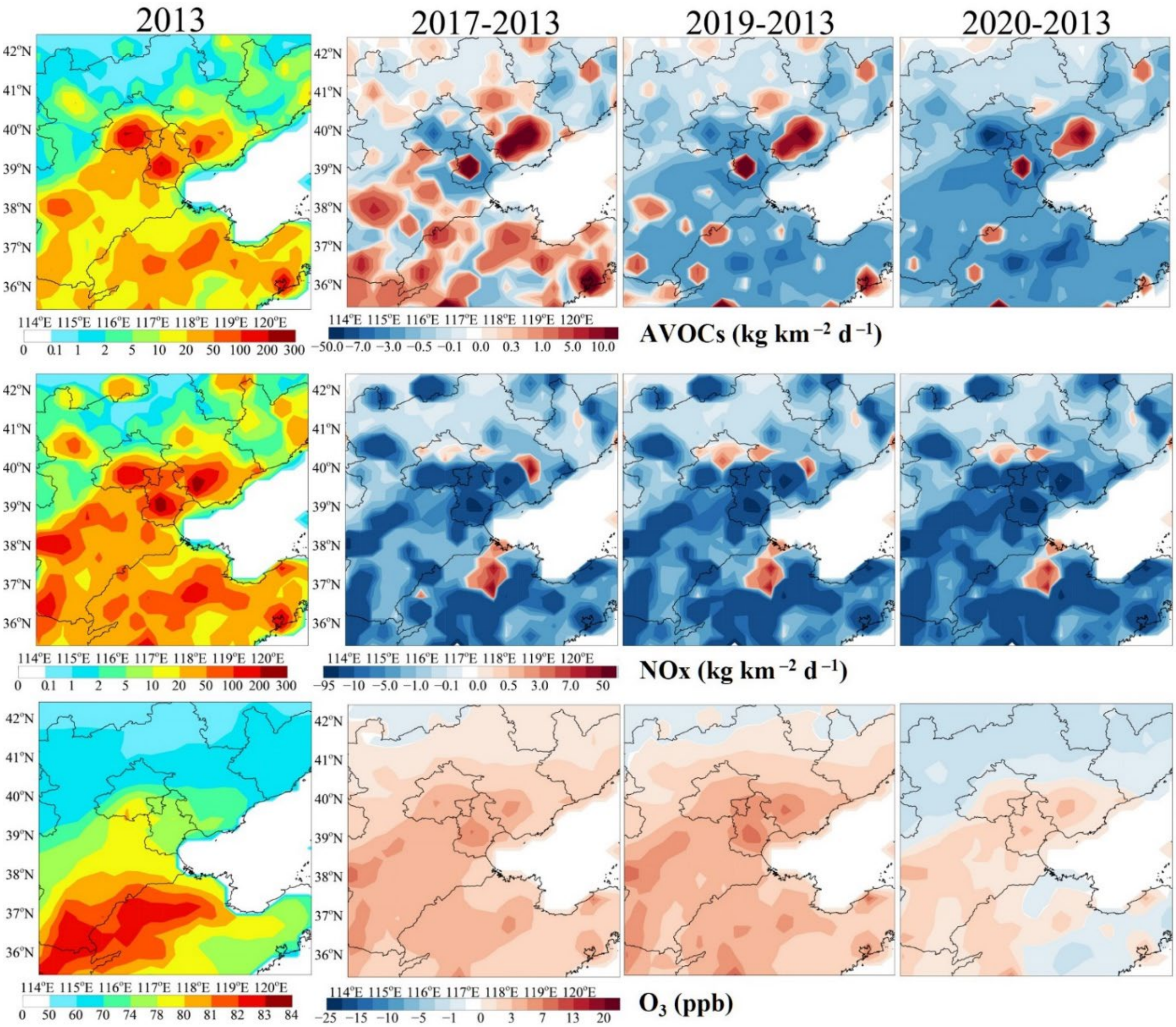

Figure 6. Summer AVOCs and NO_x emission, as well as O_3 concentration over JJJ in 2013 and its differences relative to 2013 in 2017, 2019 and 2020.

Suburban JJJ followed a different pathway. Suburban areas, mainly located in the northern part of the region, shifted gradually from transitional to NOx-limited conditions, with about 76% of suburban areas becoming NOx-limited by 2020. As this NOx-limited area expanded, the effect of Anth changed from enhancement in 2019 to suppression in 2020. In 2019, a larger fraction of suburban areas remained transitional, and increases in AVOCs under relatively stable NOx conditions promoted O_3 production. In 2020, more extensive NOx-limited conditions meant that concurrent reductions in NOx and AVOCs suppressed O_3 formation. This contrast shows that even within the same region, similar emission changes can have different effects depending on the urban–suburban evolution of O_3 sensitivity. Notably, the contribution of Anth in JJJ was

https://doi.org/10.5194/egusphere-2026-4328
Preprint. Discussion started: 24 August 2026

substantially greater than the eastern China average, reflecting the more aggressive emission reduction measures implemented in this region (Xiao et al., 2020).

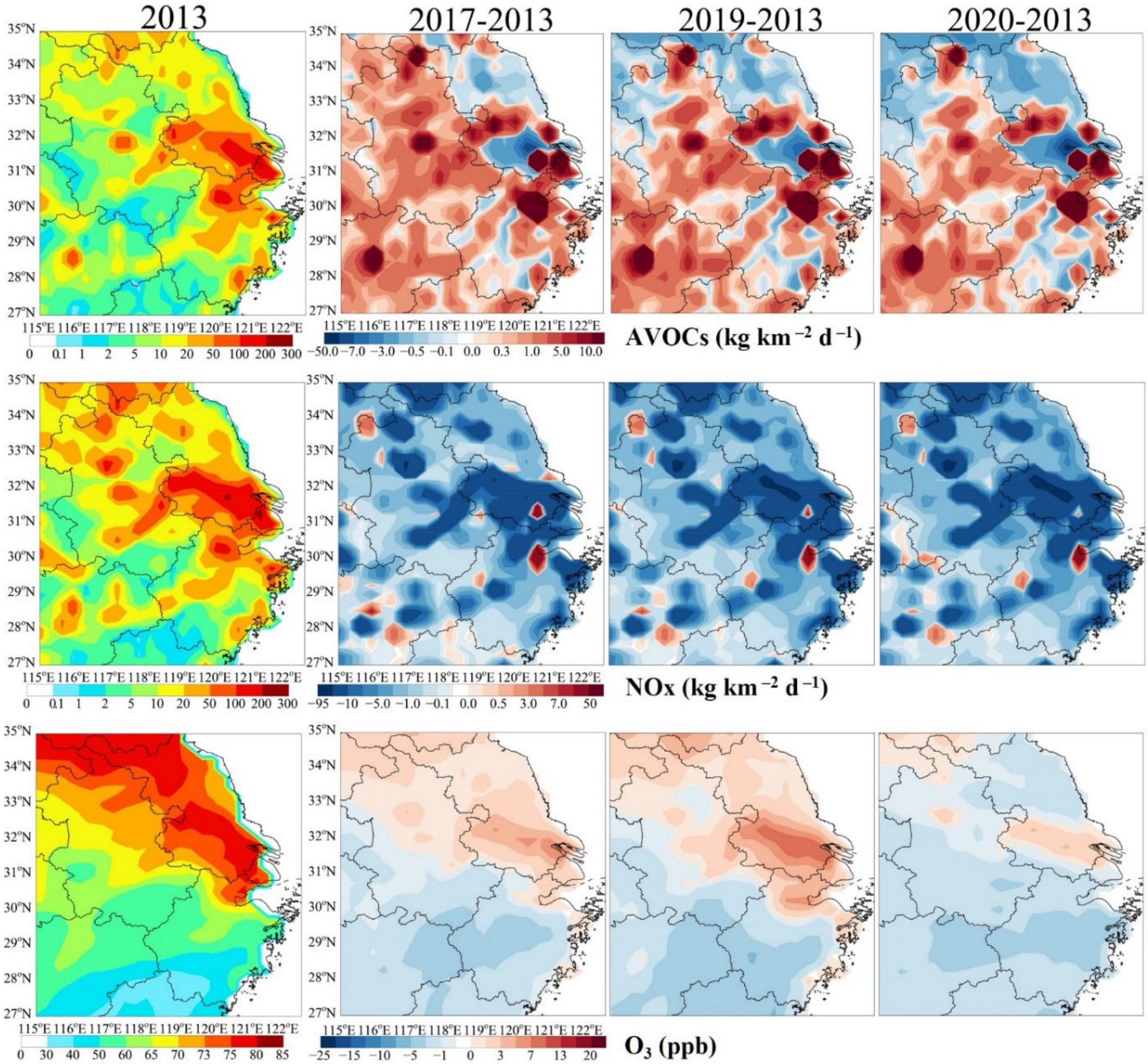

Figure 7. Summer AVOCs and NO_x emission, as well as O_3 concentration over YRD in 2013 and its differences relative to 2013 in 2017, 2019 and 2020.

The YRD exhibited another pattern as shown in Fig. 5. Suburban areas in the southern YRD were persistently NOx-limited throughout the study period, so NOx emission reductions consistently suppressed O_3 formation. In contrast, VOCs-limited regimes were mainly distributed in urbanized parts of southern Jiangsu, southeastern Anhui, and the Jiangsu–Zhejiang border region. During 2013–2017, increases in AVOCs and BVOCs together with declining NOx (Fig. 7) shifted some VOCs-limited areas toward transitional conditions. However, in 2019 and 2020, parts of the Jiangsu–Zhejiang border,

https://doi.org/10.5194/egusphere-2026-4328
Preprint. Discussion started: 24 August 2026

northern Anhui, and northern Jiangsu shifted from transitional back to VOCs-limited conditions because NOx reductions exceeded VOC increases. In these newly or persistently VOCs-limited urban areas, increased AVOCs and decreased NOx enhanced O_3 production, whereas in suburban YRD, which remained predominantly NOx-limited, NOx emission reductions controlled the O_3 response in 2017, 2019, and 2020 and led to a suppressing effect of Anth on O_3 formation.

Meteorological effects also showed strong spatial heterogeneity. Although Met often had the same sign when averaged over broad urban or suburban regions, its local influence differed between JJJ and YRD. Relative to 2013, Met suppressed O_3 in JJJ in 2017 but enhanced O_3 in YRD, highlighting the sensitivity of O_3 attribution to regional meteorological conditions. This contrast highlights the pronounced spatial heterogeneity in Met influences on O_3 pollution. Such heterogeneity means that Met can amplify or offset the effects of emission changes, particularly in suburban areas where meteorology and transport exert stronger control over regional mean O_3.

Together, these case studies show that urban–suburban O_3 trends are shaped by the combined effects of driver contributions and chemical-regime evolution. Urban areas, especially in eastern China, often shifted between VOCs-limited and transitional regimes, causing Anth to either enhance or suppress O_3 depending on the period and region. Suburban areas were more frequently NOx-limited, particularly in YRD and increasingly in JJJ. Therefore, NOx reductions generally suppressed O_3, although BVOCs and AVOCs changes could still enhance O_3 where transitional conditions persisted. Overall, the same anthropogenic emission reductions can either increase or decrease O_3 depending on whether the affected area is urban or suburban and how its O_3 formation sensitivity evolves over time.

4 Conclusion

This study investigated the evolution of summertime urban–suburban O_3 contrasts in China during 2013–2020 by combining surface observations with GEOS-Chem simulations. A key finding is that the inferred urban–suburban O_3 contrast depends strongly on how urban and suburban areas are defined. Using a population density-based classification, many monitoring sites originally labeled as suburban in developed eastern regions were reassigned to urban areas, while several originally urban sites in western China were reassigned to suburban areas. This reclassification substantially changed the estimated concentration levels, trends, and urban–suburban contrasts. In eastern China, it enlarged the urban–suburban O_3 gap by reducing the influence of urbanized sites within the suburban category. In western China, it changed the interpretation from an apparent urban O_3 exceedance under the original classification to a persistent suburban O_3 enhancement with a narrowing gap. These results demonstrate that the classification threshold is not a technical detail, but a central factor in interpreting urban–suburban O_3 differences and reconciling discrepancies among previous studies.

The representativeness of suburban monitoring sites is another important source of uncertainty. Although the model reproduced the observed interannual variability of O_3 reasonably well, simulated suburban trends were higher than site-based observations, especially in eastern China. Comparisons between site-averaged and regional grid-cell-averaged model results indicate that this discrepancy is largely related to sparse and uneven suburban monitoring coverage. Urban monitoring sites

https://doi.org/10.5194/egusphere-2026-4328
Preprint. Discussion started: 24 August 2026

were relatively representative of broader urban conditions, whereas suburban sites failed to capture the stronger spatial heterogeneity of suburban areas, which are co-influenced by BVOCs emissions, land-cover variability, regional transport, and gradients in anthropogenic emissions. As a result, site-based analyses may overestimate or misrepresent urban–suburban trend differences. Regional mean concentrations were therefore used for subsequent attribution analyses, highlighting the need for denser and more representative suburban O_3 monitoring networks.

The urban–suburban O_3 contrast showed clear temporal and regional evolution. At the national scale, O_3 increased more rapidly in suburban areas than in urban areas during 2017–2020, reducing the urban–suburban difference from 9.6 ppb in 2013 to 6.8 ppb in 2020. In eastern China, urban O_3 remained higher than suburban O_3, but faster suburban growth narrowed the gap. In western China, suburban O_3 remained higher than urban O_3, and faster suburban growth strengthened the suburban enhancement. Attribution results further show that meteorology, anthropogenic emissions, and BVOCs emissions affected urban and suburban O_3 differently. In eastern urban areas, anthropogenic emission changes enhanced O_3 during 2013–2017 under VOCs-limited conditions, but their effect weakened and became negative by 2020 as O_3 formation shifted toward transitional conditions. In eastern suburban areas, O_3 formation remained predominantly NOx-limited, so anthropogenic emission reductions consistently suppressed O_3, while meteorology was the dominant driver of O_3 variability. In western China, weak anthropogenic and BVOCs emissions made meteorology the primary control in both urban and suburban areas.

The contrasting behavior of urban and suburban O_3 is ultimately linked to differences in O_3 formation sensitivity and its evolution. Case studies of the JJJ and YRD regions show that urban areas were more likely to experience shifts between VOCs-limited and transitional regimes, causing anthropogenic emission changes to enhance or suppress O_3 depending on the period and location. By contrast, suburban areas were more frequently NOx-limited, particularly in the YRD and increasingly in the JJJ region, making NOx reductions more likely to suppress O_3. BVOCs emissions were not the dominant driver at the regional mean scale. Overall, the same emission reduction can produce different, or even opposite, O_3 responses in urban and suburban environments depending on local chemical sensitivity. Effective O_3 mitigation in China therefore requires spatially differentiated strategies that account for urban–suburban classification, monitoring representativeness, meteorological variability, and the evolving O_3 formation regime.

Code and data availability

The code and data supporting the conclusions of this paper are available from https://doi.org/10.5281/zenodo.21429805 (Yang, 2026).

https://doi.org/10.5194/egusphere-2026-4328
Preprint. Discussion started: 24 August 2026

Author contributions

QW conceptualized and designed the study. QW and NY prepared the initial draft of the manuscript. NY performed the model simulations and conducted the formal data analysis. GL, ZY, YZ, and ZH also contributed to the model simulations. QW, NY, and NM revised and refined the manuscript. All authors contributed to the scientific discussion, reviewed the manuscript, and approved the final version.

Competing interests

At least one of the (co-)authors is a member of the editorial board of Atmospheric Chemistry and Physics.

Disclaimer

Publisher's note: Copernicus Publications remains neutral with regard to jurisdictional claims made in the text, published maps, institutional affiliations, or any other geographical representation in this paper. While Copernicus Publications makes every effort to include appropriate place names, the final responsibility lies with the authors. Views expressed in the text are those of the authors and do not necessarily reflect the views of the publisher.

Acknowledgements

We thank for the technical support of the National Large Scientific and Technological Infrastructure "Earth System Numerical Simulation Facility" (https://cstr.cn/31134.02.EL). We also gratefully acknowledge the China National Environmental Monitoring Centre (CNEMC) for providing the nationwide surface ozone observations used in this study.

Financial support

The work was supported by the special fund of the National Key R&D Program of China (2024YFC3712902), National Natural Science Foundation of China (42377093), and the Guangdong Basic and Applied Basic Research Foundation (2024B1515040026).

https://doi.org/10.5194/egusphere-2026-4328
Preprint. Discussion started: 24 August 2026

References

Andreae, M. O.: Emission of trace gases and aerosols from biomass burning–an updated assessment, Atmos. Chem. Phys., 19, 8523-8546, https://doi.org/10.5194/acp-19-8523-2019, 2019.

Cao, J., Situ, S., Hao, Y., Xie, S., and Li, L.: Enhanced summertime ozone and SOA from biogenic volatile organic compound (BVOC) emissions due to vegetation biomass variability during 1981–2018 in China, Atmos Chem Phys, 22, 2351-2364, https://doi.org/10.5194/acp-22-2351-2022, 2022.

Dai, H., Liao, H., Wang, Y., and Qian, J.: Co-occurrence of ozone and $PM_{2.5}$ pollution in urban/non-urban areas in eastern China from 2013 to 2020: Roles of meteorology and anthropogenic emissions, Sci Total Environ, 924, 171687, https://doi.org/10.1016/j.scitotenv.2024.171687, 2024.

Gao, C., Zhang, X., Lun, X., Gao, Y., Guenther, A., Zhao, H., Zhang, S., Huang, L., Song, K., Huang, X., Gao, M., Ma, P., Jia, Z., Xiu, A., and Zhang, Y.: BVOCs' role in dynamic shifts of summer ozone formation regimes across China and policy implications, Journal of Environmental Management, 376, 124150, https://doi.org/10.1016/j.jenvman.2025.124150, 2025.

Gao, L., Yue, X., Meng, X., Du, L., Lei, Y., Tian, C., and Qiu, L.: Comparison of ozone and $PM_{2.5}$ concentrations over urban, suburban, and background sites in China, Adv. Atmos. Sci., 37, 1297-1309, https://doi.org/10.1007/s00376-020-0054-2, 2020.

Geng, G., Liu, Y., Liu, Y., Liu, S., Cheng, J., Yan, L., Wu, N., Hu, H., Tong, D., Zheng, B., Yin, Z., He, K., and Zhang, Q.: Efficacy of China's clean air actions to tackle $PM_{2.5}$ pollution between 2013 and 2020, Nat Geosci, 17, 987-994, https://doi.org/10.1038/s41561-024-01540-z, 2024.

Giglio, L., Randerson, J. T., and van der Werf, G. R.: Analysis of daily, monthly, and annual burned area using the fourth-generation global fire emissions database (GFED4), J Geophys Res-Biogeo, 118, 317-328, https://doi.org/10.1002/jgrg.20042, 2013.

Guenther, A. B., Jiang, X., Heald, C. L., Sakulyanontvittaya, T., Duhl, T., Emmons, L. K., and Wang, X.: The Model of Emissions of Gases and Aerosols from Nature version 2.1 (MEGAN2.1): an extended and updated framework for modeling biogenic emissions, Geosci Model Dev, 5, 1471-1492, https://doi.org/10.5194/gmd-5-1471-2012, 2012.

Guo, H., Chen, K., Wang, P., Hu, J., Ying, Q., Gao, A., and Zhang, H.: Simulation of summer ozone and its sensitivity to emission changes in China, Atmos Pollut Res, 10, 1543-1552, https://doi.org/https://doi.org/10.1016/j.apr.2019.05.003, 2019.

Guo, L., Wang, X., Baklanov, A., and Shao, M.: $PM_{2.5}$ Concentration Gap Reduction between Typical Urban and Nonurban China from 2000 to 2023, ACS ES&T Air, 2, 90-98, https://doi.org/10.1021/acsestair.4c00208, 2024.

Hoesly, R. M., Smith, S. J., Feng, L., Klimont, Z., Janssens-Maenhout, G., Pitkanen, T., Seibert, J. J., Vu, L., Andres, R. J., Bolt, R. M., Bond, T. C., Dawidowski, L., Kholod, N., Kurokawa, J.-i., Li, M., Liu, L., Lu, Z., Moura, M. C. P., O'Rourke, P. R., and Zhang, Q.: Historical (1750–2014) anthropogenic emissions of reactive gases and aerosols from the Community Emissions Data System (CEDS), Geosci Model Dev, 11, 369-408, https://doi.org/10.5194/gmd-11-369-2018, 2018.

Jin, X., Fiore, A., Boersma, K. F., Smedt, I. D., and Valin, L.: Inferring Changes in Summertime Surface Ozone–NOx–VOC Chemistry over U.S. Urban Areas from Two Decades of Satellite and Ground-Based Observations, Environmental Science & Technology, 54, 6518-6529, https://doi.org/10.1021/acs.est.9b07785, 2020.

Li, J., Wang, H., Gong, D., Li, Q., Wang, Y., Zhao, W., Zhang, C., Zhou, Z., Zhao, Y., Xu, Q., Zhou, Y., He, C., Ristovski, Z., Morawska, L., Liu, S. C., and Wang, B.: Landscape fragmentation triggers cascading enhancement of surface ozone production, Communications Earth & Environment, 6, 931, https://doi.org/10.1038/s43247-025-02866-1, 2025.

Li, K., Jacob, D. J., Liao, H., Shen, L., Zhang, Q., and Bates, K. H.: Anthropogenic drivers of 2013–2017 trends in summer surface ozone in China, Proc. Natl. Acad. Sci. U.S.A., 116, 422-427, https://doi.org/10.1073/pnas.1812168116, 2019.

Li, K., Jacob, D. J., Shen, L., Lu, X., De Smedt, I., and Liao, H.: Increases in surface ozone pollution in China from 2013 to 2019: anthropogenic and meteorological influences, Atmos Chem Phys, 20, 11423-11433, https://doi.org/10.5194/acp-20-11423-2020, 2020.

Li, R., Xu, M., Li, M., Chen, Z., Zhao, N., Gao, B., and Yao, Q.: Identifying the spatiotemporal variations in ozone formation regimes across China from 2005 to 2019 based on polynomial simulation and causality analysis, Atmos Chem Phys, 21, 15631-15646, https://doi.org/10.5194/acp-21-15631-2021, 2021.

https://doi.org/10.5194/egusphere-2026-4328
Preprint. Discussion started: 24 August 2026

Liu, Y. and Wang, T.: Worsening urban ozone pollution in China from 2013 to 2017–Part 2: The effects of emission changes and implications for multi-pollutant control, Atmos. Chem. Phys., 20, 6323-6337, https://doi.org/10.5194/acp-20-6323-2020, 2020.

Liu, Y., Geng, G., Cheng, J., Liu, Y., Xiao, Q., Liu, L., Shi, Q., Tong, D., He, K., and Zhang, Q.: Drivers of increasing ozone during the two phases of clean air actions in China 2013–2020, Environmental Science & Technology, 57, 8954-8964, https://doi.org/10.1021/acs.est.3c00054, 2023.

Pye, H. O. T., Chan, A. W. H., Barkley, M. P., and Seinfeld, J. H.: Global modeling of organic aerosol: the importance of reactive nitrogen (NO_X and NO_3), Atmos. Chem. Phys., 10, 11261-11276, https://doi.org/10.5194/acp-10-11261-2010, 2010.

Wang, H., Yu, X., Luo, L., and Li, R.: Urban–Rural Boundary Delineation Based on Population Spatialization: A Case Study of Guizhou Province, China, Sustainability-Basel, 16, 1787, https://doi.org/10.3390/su16051787, 2024.

Wang, H., Huang, C., Tao, W., Gao, Y., Wang, S., Jing, S., Wang, W., Yan, R., Wang, Q., An, J., Tian, J., Hu, Q., Lou, S., Pöschl, U., Cheng, Y., and Su, H.: Seasonality and reduced nitric oxide titration dominated ozone increase during COVID-19 lockdown in eastern China, Npj Clim Atmos Sci, 5, 24, https://doi.org/10.1038/s41612-022-00249-3, 2022a.

Wang, T., Xue, L. K., Brimblecombe, P., Lam, Y. F., Li, L., and Zhang, L.: Ozone pollution in China: A review of concentrations, meteorological influences, chemical precursors, and effects, Sci Total Environ, 575, 1582-1596, https://doi.org/10.1016/j.scitotenv.2016.10.081, 2017.

Wang, W., van der A, R., Ding, J., van Weele, M., and Cheng, T.: Spatial and temporal changes of the ozone sensitivity in China based on satellite and ground-based observations, Atmos Chem Phys, 21, 7253-7269, https://doi.org/10.5194/acp-21-7253-2021, 2021.

Wang, W., Parrish, D. D., Wang, S., Bao, F., Ni, R., Li, X., Yang, S., Wang, H., Cheng, Y., and Su, H.: Long-term trend of ozone pollution in China during 2014–2020: distinct seasonal and spatial characteristics and ozone sensitivity, Atmos. Chem. Phys., 22, 8935-8949, https://doi.org/10.5194/acp-22-8935-2022, 2022b.

Wu, K., Yang, X. Y., Chen, D., Gu, S., Lu, Y. Q., Jiang, Q., Wang, K., Ou, Y. H., Qian, Y., Shao, P., and Lu, S. H.: Estimation of biogenic VOC emissions and their corresponding impact on ozone and secondary organic aerosol formation in China, Atmos Res, 231, https://doi.org/10.1016/j.atmosres.2019.104656, 2020.

Xiao, Q., Geng, G., Liang, F., Wang, X., Lv, Z., Lei, Y., Huang, X., Zhang, Q., Liu, Y., and He, K.: Changes in spatial patterns of $PM_{2.5}$ pollution in China 2000–2018: Impact of clean air policies, Environment International, 141, 105776, https://doi.org/10.1016/j.envint.2020.105776, 2020.

Xing, L., Mao, X., and Duan, K.: Impacts of urban–rural disparities in the trends of $PM_{2.5}$ and ozone levels in China during 2013–2019, Atmos. Pollut. Res., 13, 101590, https://doi.org/10.1016/j.apr.2022.101590, 2022.

Xu, J., Silver, B., Tang, R., Wang, N., Huang, X., Ding, A., and Arnold, S. R.: A model assessment of the relationship between urban greening and ozone air quality in China: a study of three metropolitan regions, Npj Clim Atmos Sci, 8, 184, https://doi.org/10.1038/s41612-025-01054-4, 2025.

Xue, L., Zhu, Y., Gao, J., Zhong, X., Cui, C., Wang, S., Jiang, Z., Sun, Y., Li, Q., Zhang, Y., Li, H., Zhang, Y., Wang, S., Zhao, M., Shen, H., Zhang, Y., Tang, G., Wang, T., and Wang, W.: Critical transition of urban ozone formation regime in the North China Plain, Natl Sci Rev, 13, https://doi.org/10.1093/nsr/nwaf596, 2026.

Yan, D., Jin, Z., Zhou, Y., Li, M., Zhang, Z., Wang, T., Zhuang, B., Li, S., and Xie, M.: Anthropogenically and meteorologically modulated summertime ozone trends and their health implications since China's clean air actions, Environmental Pollution, 343, 123234, https://doi.org/10.1016/j.envpol.2023.123234, 2024.

Yang, N., Wang, Q., Xiong, Q., Fan, Z., Liu, G., Li, F., Zhu, S., Zhou, Y., Tao, J., Hong, J., Wang, H., Huang, C., Sun, Y., Cheng, Y., Su, H., and Ma, N.: Intermediate-Volatility Organic Compounds (IVOCs) Emissions Based on Source-Specific Emission Ratios Relative to NonMethane Volatile Organic Compounds (NMVOCs) Give Better Representation of the Spatial Distribution of IVOCs in China, J Geophys Res-Atmos, 130, https://doi.org/10.1029/2024JD041464, 2025.

Yang, X., Zhang, G., Sun, Y., Zhu, L., Wei, X., Li, Z., and Zhong, X.: Explicit modeling of background HCHO formation in southern China, Atmos Res, 240, 104941, https://doi.org/10.1016/j.atmosres.2020.104941, 2020.

Zhang, Q., Zheng, Y., Tong, D., Shao, M., Wang, S., Zhang, Y., Xu, X., Wang, J., He, H., Liu, W., Ding, Y., Lei, Y., Li, J., Wang, Z., Zhang, X., Wang, Y., Cheng, J., Liu, Y., Shi, Q., Yan, L., Geng, G., Hong, C., Li, M., Liu, F., Zheng, B., Cao, J., Ding, A., Gao, J., Fu, Q., Huo, J., Liu, B., Liu, Z., Yang, F., He, K., and Hao, J.: Drivers of improved $PM_{2.5}$ air quality

https://doi.org/10.5194/egusphere-2026-4328
Preprint. Discussion started: 24 August 2026

in China from 2013 to 2017, Proc. Natl. Acad. Sci. U.S.A., 116, 24463-24469, https://doi.org/10.1073/pnas.1907956116, 2019.

Zheng, B., Tong, D., Li, M., Liu, F., Hong, C., Geng, G., Li, H., Li, X., Peng, L., Qi, J., Yan, L., Zhang, Y., Zhao, H., Zheng, Y., He, K., and Zhang, Q.: Trends in China's anthropogenic emissions since 2010 as the consequence of clean air actions, Atmos. Chem. Phys., 18, 14095-14111, https://doi.org/10.5194/acp-18-14095-2018, 2018.

Zheng, H., Kong, S., He, Y., Song, C., Cheng, Y., Yao, L., Chen, N., and Zhu, B.: Enhanced ozone pollution in the summer of 2022 in China: The roles of meteorology and emission variations, Atmos Environ, 301, 119701, https://doi.org/https://doi.org/10.1016/j.atmosenv.2023.119701, 2023.